Istituto
Nazionale
Fisica
Nucleare

Sezione SANITÀ
Istituto Superiore di Sanità
Viale Regina Elena 299
I-00161 Roma, Italy

INFN-ISS 96/11
December 1996

Neutron electromagnetic form factors and inclusive scattering of polarized electrons by polarized ^{3}He and ^{3}H targets

A. Kievsky[1], E. Pace[2], G. Salmè[3], M. Viviani[1]

[1] *INFN, Sezione di Pisa, 56010 S.Piero a Grado, Pisa, Italy*

[2] *Dipartimento di Fisica, Università di Roma "Tor Vergata", and INFN, Sezione Tor Vergata, Via della Ricerca Scientifica 1, I-00133 Roma, Italy*

[3] *INFN, Sezione Sanità, Viale Regina Elena 299, I-00161 Roma, Italy*

Abstract

The electromagnetic inclusive responses of polarized ^{3}He and ^{3}H are thoroughly investigated at the quasielastic peak for squared momentum transfers up to 2 $(GeV/c)^2$, within the plane wave impulse approximation. Great emphasys is put on the effects in the bound-state due to different two- and three-body nuclear forces, and to the Coulomb interaction as well. A careful analysis of the polarized responses allows to select possible experiments for minimizing the model dependence in the extraction of the neutron electromagnetic form factors. In particular, the relevant role played by the proton in the transverse-longitudinal response of polarized ^{3}He, at low momentum transfer, can be utilized for obtaining valuable information on the proton contribution to the total polarized response and eventually on the neutron charge form factor.

PACS: 25.30.-c,24.70.+s,25.10.+s,29.25.pg

To appear in **Phys. Rev. C**

1. Introduction

The relevance of an accurate knowledge of nucleon electromagnetic (em) form factors is well known, and this fact has motivated an impressive amount of experimental work for investigating these observables. A particularly difficult problem is represented by the extraction of the neutron em form factors, since free neutron targets do not exist in nature, and therefore one is forced to consider nucleon bound systems, such as deuteron (see e.g. [1]) or polarized ^{3}He [2]. In the latter case, within a naive model, with only a symmetric S-wave component in the bound-state, the two protons have opposite spins and therefore one should expect that the em polarized response of ^{3}He essentially is the neutron one. Unfortunately, the presence of components with other symmetries, e.g. the S'-wave, and higher angular momenta, e.g. the D-wave, prevents the application of the naive picture and therefore also the polarized ^{3}He target is plagued by a non negligible proton contribution. In spite of this, many experimental efforts [3, 4, 5, 6] have been carried out with the aim of measuring the inclusive response of polarized ^{3}He at the quasielastic (qe) peak. Though such measurements were affected by sizable statistical and systematic uncertainties, a first estimate of the neutron magnetic form factor at $Q^2 \approx 0.2$ $(GeV/c)^2$ [5] was extracted from the transverse polarized response (with a $\approx$ 20% accuracy), while no information on the charge form factor could be reliably obtained [6], due to the large proton contribution in the transverse-longitudinal polarized response. In order to improve the accuracy, in particular for the transverse polarized response, a new generation of inclusive experiments to be performed in the near future at TJNAF has been planned (see e.g. [7]). On the theoretical side, the inclusive polarized responses have been analyzed within the *plane wave impulse approximation* (PWIA), by calculating the spin-dependent spectral function of ^{3}He [8, 9] from realistic wave functions of the three-nucleon system, pointing out the unpleasant presence of the proton contribution, particularly in the transverse-longitudinal response investigated in the experiments of Refs. [3, 4, 6]. Nevertheless, a suitable choice of the polarization angle can minimize the proton contribution, as discussed in detail in [8]. It is worth noting that i) the inclusion of the final state interaction (FSI), between the knocked out nucleon and the spectator pair, ii) the meson exchange currents, iii) the relativistic corrections and iv) the presence of the Δ in the bound-state, are still open problems for the inclusive polarized responses of the three-nucleon system. As far as the first topic is concerned, that only for unpolarized cross sections refined calculations including FSI are available [10, 11], exhibiting large FSI effects at very low momentum transfer ($Q^2 < 0.1$ $(GeV/c)^2$), while at $Q^2 > 0.25$ $(GeV/c)^2$ PWIA calculations are able to give a good description of the experimental data at the qe peak, both for the unpolarized longitudinal and transverse response functions [12, 13].

Our aim is to study, within the PWIA, em inclusive polarized responses of both ^{3}He and ^{3}H, at the qe peak, for a wide range of momentum transfer, in order to explore the model dependence due to the initial state interaction (ISI) (see also [6] for the particular case of the corresponding experiment). We have obtained the spin-dependent spectral function from bound-state wave functions, calculated using the Pair correlated Hyperspherical-Harmonic (PHH) basis [14] and different realistic two- and three-body nuclear forces; moreover, we

have also considered the Coulomb interaction in ^{3}He. After a detailed analysis of the effects of two- and three-body interactions on the polarized responses, we have singled out possible experiments for minimizing the model dependence due to both the nuclear structure and the presence of the proton contribution, when neutron form factors are extracted. First of all, we propose a measurement of the transverse-longitudinal polarized response of ^{3}He at low momentum transfer, in the range $0.1 \leq Q^2 \leq 0.3$ $(GeV/c)^2$, since one could obtain valuable information on the proton contribution to this response, just taking advantage of the proton predominance in this kinematical region. Moreover, a measurement of the polarization angle where the proton contribution to the polarized cross section is vanishining, could give the ratio between the proton contributions to the transverse response and the transverse-longitudinal one; it will be pointed out that an estimate of such a polarization angle can be obtained through a measurement of protons emitted along the direction of the three-momentum transfer. Finally, future experiments for measuring the em response of polarized ^{3}H could close the chain for obtaining an almost model independent extraction of both electric and magnetic neutron form factors.

The paper is organized as follows: in Sect. 2, the inclusive cross section of polarized electrons by a polarized three-nucleon target will be reported, as well as the nuclear polarized response functions obtained within the PWIA; in Sect. 3, the three-nucleon ground-state and the spin-dependent spectral functions we have adopted will be illustrated in detail; in Sect. 4, the comparison between our results, calculated by using different realistic two- and three-body interactions, and the most recent experimental values for ^{3}He asymmetries [5, 6] will be presented, and em polarized responses at qe peak, for both ^{3}He and ^{3}H, will be investigated in detail up to $Q^2 = 2$ $(GeV/c)^2$; in Sect. 5, possible experiments for minimizing the model dependence in the extraction of neutron em form factors will be suggested; in Sect. 6 conclusions will be drawn.

2. The inclusive cross section and the em responses of a J = 1/2 nucleus

In this Section the PWIA formalism we have adopted will be presented, with a particular emphasysis on the em responses in terms of the spin-dependent spectral function of the three-body system.

First of all, the inclusive cross section of a longitudinally polarized electron with helicity $h = \pm 1$ from a $J = 1/2$ nucleus is reported for the sake of completeness. After contracting the em tensors for the electron and for the nuclear target, A, the cross section can be cast in terms of the unpolarized (R_L^A, R_T^A) and polarized ($R_{T'}^A$, $R_{TL'}^A$) nuclear response functions as follows (for a detailed discussion see [8], cf. also [9, 15])

$$\frac{d^2\sigma(h)}{d\Omega_2 d\nu} \; = \; \Sigma \; + \; h \; \Delta \tag{1}$$

with

$$\Sigma \;=\; \sigma_{Mott}\left[\left(\frac{Q^2}{|\vec{q}|^2}\right)^2 R_L^A(Q^2,\nu) \;+\; \left(\frac{Q^2}{2|\vec{q}|^2}+tan^2\frac{\theta_e}{2}\right)\; R_T^A(Q^2,\nu)\right] \tag{2}$$

$$\Delta \;=\; -\,\sigma_{Mott}\; tan\frac{\theta_e}{2}\left\{cos\theta^*\; R_{T'}^A(Q^2,\nu)\;\left[\frac{Q^2}{|\vec{q}|^2}+tan^2\frac{\theta_e}{2}\right]^{1/2} \;+\right.$$
$$\left. -\;\frac{Q^2}{|\vec{q}|^2\;\sqrt{2}}\; sin\theta^* cos\phi^*\; R_{TL'}^A(Q^2,\nu)\right\} \tag{3}$$

where θ_e is the scattering angle; θ^* and ϕ^* are the azimuthal and polar angles of the target polarization vector $\vec{S}_A$, with respect to the direction of the three-momentum transfer $\vec{q}$; $Q^2 = |\vec{q}|^2 - \nu^2$. In our analysis, in addition to θ^*, another polarization angle, β, will be used, defined with respect to the direction of the incoming electron beam, i.e. $cos\beta \equiv \vec{S}_A \cdot \vec{k}_1/|\vec{k}_1|$, where $\vec{k}_{1(2)}$ is the three-momentum of the initial (final) electron. The relation between the polarization angles we have considered is

$$cos\theta^* = \frac{\epsilon_1\; cos\beta \;-\; \epsilon_2\;(sin\beta\; sin\theta_e\; cos\phi \;+\; cos\beta\; cos\theta_e)}{|\vec{q}|}$$
$$sin\theta^* cos\phi^* = \frac{|\vec{q}|cos\beta \;-(\epsilon_1 \;-\; \epsilon_2 cos\theta_e)cos\theta^*}{\epsilon_2 sin\theta_e} \tag{4}$$

where ϕ is the polar angle with respect to $\vec{k}_1/|\vec{k}_1|$. In the case of coplanar kinematics (i.e. $\phi = 0^o\;,\; 180^o$) one can have only $\phi^* = 0^o$ or 180^o.

Following [8], the nuclear response functions can be expressed in terms of a 2x2 matrix $\hat{\mathbf{P}}^N_{\mathcal{M}}(\vec{p},E)$ representing the spin dependent spectral function of a nucleon, N, inside a nucleus with component of the total angular momentum along the polarization $\vec{S}_A$ equal to $\mathcal{M}$. The elements of the matrix $\hat{\mathbf{P}}^N_{\mathcal{M}}(\vec{p},E)$ are given by

$$P^N_{\sigma,\sigma',\mathcal{M}}(\vec{p},E) = \sum_{f_{(A-1)}} \;{}_N\langle\vec{p},\sigma;\psi_{f_{(A-1)}}|\psi_{J\mathcal{M}}\rangle\;\langle\psi_{J\mathcal{M}}|\psi_{f_{(A-1)}};\vec{p},\sigma'\rangle_N\;\delta(E-E_{f_{(A-1)}}+E_A) \tag{5}$$

where $|\psi_{J\mathcal{M}}\rangle$ is the ground state of the target nucleus with polarization $\vec{S}_A$, $|\psi_{f_{(A-1)}}\rangle$ an eigenstate of the spectator system with quantum numbers f and interacting through the *same interaction* of the target nucleus, $|\vec{p},\sigma\rangle_N$ a plane wave describing the nucleon N with spin component, along the z-axis, equal to σ; E is the missing energy. In a more compact form, for $J = 1/2$, $\hat{\mathbf{P}}^N_{\mathcal{M}}(\vec{p},E)$ can be written as

$$\hat{\mathbf{P}}^N_{\mathcal{M}}(\vec{p},E) = \frac{1}{2}\left\{B^N_{0,\mathcal{M}}(|\vec{p}|,E) \;+\; \vec{\sigma}\cdot\left[\vec{S}_A\; B^N_{1,\mathcal{M}}(|\vec{p}|,E) \;+\; \hat{p}\;(\hat{p}\cdot\vec{S}_A)\; B^N_{2,\mathcal{M}}(|\vec{p}|,E)\right]\right\} \tag{6}$$

where the function $B^N_{0,\mathcal{M}}(|\vec{p}|,E)$ is the trace of $\hat{\mathbf{P}}^N_{\mathcal{M}}(\vec{p},E)$ and yields the usual unpolarized spectral function, while $B^N_{1,\mathcal{M}}(|\vec{p}|,E)$ and $B^N_{2,\mathcal{M}}(|\vec{p}|,E)$ describe the spin structure of the

probability distribution of finding a nucleon with a given momentum, missing energy and polarization. As a matter of fact the effective polarization of a nucleon is given by

$$\mathcal{P}^N = \langle \psi_{J\frac{1}{2}} | \vec{S}_A \cdot \vec{\sigma} | \psi_{J\frac{1}{2}} \rangle \; = \; \int dE \; \int d\vec{p} \; \mathbf{Tr} \left[\vec{S}_A \cdot \vec{\sigma} \; \hat{\mathbf{P}}^N_{\frac{1}{2}}(\vec{p}, E) \right] \; =$$
$$= \; 4\pi \; \int dE \; \int p^2 \; dp \; \left(B^N_{1,\frac{1}{2}}(|\vec{p}|, E) \; + \; \frac{B^N_{2,\frac{1}{2}}(|\vec{p}|, E)}{3} \right) \tag{7}$$

In Sect. 3, where more details will be given on the spin-dependent spectral function, the values of $\mathcal{P}^N$ in ^{3}He will be also presented for the different interactions we have used, but we can anticipate that $\mathcal{P}^n$ is about $86 - 87$ %, in line with the analysis of the world calculations of Ref. [16]. Explicit expressions for the functions $B_{0(1,2),\mathcal{M}}$ can be found in [8].

The evaluation of the response functions R^A_L, R^A_T, $R^A_{T'}$ and $R^A_{TL'}$ requires an off-energy-shell em nucleon tensor in the PWIA convolution formulas. In the literature different recipes for the off-energy-shell em nucleon current have been proposed (see e.g. [17, 18]). In particular, in the widely adopted prescriptions CC1 and CC2 of [17] the longitudinal component of the em current is eliminated in favour of the charge component in order to restore the current conservation (Coulomb gauge). In the actual calculations we have adopted such an approximation, since we have checked that in PWIA it allows for a good description of the accurate experimental data for the unpolarized ^{3}He longitudinal and transverse responses at $Q^2 \; > \; 0.25 \; (GeV/c)^2$ (see also [12, 13]), while the approximation, based on the elimination of the charge component in favour of the longitudinal one (Weyl gauge), underestimates the longitudinal response at the top of the qe peak (it should be pointed out that the possible FSI effects are expected to further reduce the response at the top of the qe peak [10], worsening the comparison with the data). It turns out that in the Landau gauge (i.e. $J^\mu \; \rightarrow \; J^\mu + q^\mu J \cdot q/Q^2$) the responses are essentially the same as in the Coulomb one. In the following only the expressions corresponding to the CC1 prescription are reported, since the numerical results obtained by using CC2 slightly differ (see Sect. 4). After a lengthy algebra (cf. [8] for the on-energy-shell case) one gets (in the following, $p \; \equiv \; |\vec{p}|$ and $q \; \equiv \; |\vec{q}|$)

$$R^A_L\left(Q^2, \nu\right) = \frac{\pi}{2} \sum_{N=p,n} \mathcal{N}^N_A \int_{E_{min}}^{E_{max}(Q^2,\nu)} dE \int_{p_{min}(Q^2,\nu,E)}^{p_{max}(Q^2,\nu,E)} \frac{p}{qE_p} \; dp \; B^N_0(p, E)$$
$$\left\{ (2E_p + \bar{\nu})^2 \left(\left(F^N_1\left(Q^2\right) \right)^2 + \bar{\tau} \left(F^N_2\left(Q^2\right) \right)^2 \right) - q^2 \left(F^N_1\left(Q^2\right) + F^N_2\left(Q^2\right) \right)^2 \right\} \tag{8}$$

$$R^A_T\left(Q^2, \nu\right) = \pi \sum_{N=p,n} \mathcal{N}^N_A \int_{E_{min}}^{E_{max}(Q^2,\nu)} dE \int_{p_{min}(Q^2,\nu,E)}^{p_{max}(Q^2,\nu,E)} \frac{p}{qE_p} \; dp \; B^N_0(p, E)$$

$$\left\{ \bar{Q}^2 \left(F_1^N\left(Q^2\right) + F_2^N\left(Q^2\right)\right)^2 + 2p^2 sin^2\alpha \left(\left(F_1^N\left(Q^2\right)\right)^2 + \bar{\tau} \left(F_2^N\left(Q^2\right)\right)^2 \right) \right\} \qquad (9)$$

$$R^A_{T'}\left(Q^2,\nu\right) = 2\pi \sum_{N=p,n} \mathcal{N}_A^N \left(F_1^N\left(Q^2\right) + F_2^N\left(Q^2\right)\right) \int_{E_{min}}^{E_{max}(Q^2,\nu)} dE \int_{p_{min}(Q^2,\nu,E)}^{p_{max}(Q^2,\nu,E)} \frac{p}{qE_p}\, dp$$

$$\left\{ p\ cos\alpha \ \left(B_1^N(p,E) \ + B_2^N(p,E)\right) \left[\left(F_1^N\left(Q^2\right) - F_2^N\left(Q^2\right) \frac{\bar{Q}^2}{2M\bar{\nu}} \right) \frac{\bar{\nu} p\ cos\alpha}{M+E_p} - \ F_1^N\left(Q^2\right) q \right] \ + \right.$$

$$\left. + \ \left(B_1^N(p,E) \ + B_2^N(p,E)\, cos^2\alpha \right) \ M\bar{\nu} \ \left(F_1^N\left(Q^2\right) + F_2^N\left(Q^2\right) \frac{\bar{Q}^2 E_p}{2M^2\bar{\nu}} \right) \right\} \qquad (10)$$

$$R^A_{TL'}\left(Q^2,\nu\right) = -\sqrt{2}\ q\ 2\pi \sum_{N=p,n} \mathcal{N}_A^N \left(F_1^N\left(Q^2\right) + F_2^N\left(Q^2\right)\right) \int_{E_{min}}^{E_{max}(Q^2,\nu)} dE \int_{p_{min}(Q^2,\nu,E)}^{p_{max}(Q^2,\nu,E)} \frac{p}{qE_p}\, dp$$

$$\left\{ \left(B_1^N(p,E) \ + B_2^N(p,E)\right) \left(F_1^N\left(Q^2\right) + F_2^N\left(Q^2\right) \frac{\bar{\nu}}{2M} \right) \frac{p^2\ sin^2\alpha}{2(M+E_p)} \ + \right.$$

$$+ \ F_2^N\left(Q^2\ \right) \frac{p\ cos\alpha}{2M}\ qB_1^N(p,E) +$$

$$\left. + \ \left(B_1^N(p,E) \ + \frac{B_2^N(p,E)}{2} sin^2\alpha \right) M \ \left(F_1^N\left(Q^2\right) - F_2^N\left(Q^2\right) \frac{\bar{\nu} E_p}{2M^2} \right) \right\} \qquad (11)$$

where $B^N_{0(1,2)} \equiv B^N_{0(1,2),\frac{1}{2}}$ are the functions corresponding to the target nucleus, $F^N_{1(2)}$ is the Dirac (Pauli) nucleon form factor, $\mathcal{N}_A^{p(n)}$ the number of proton (neutron) in the nucleus A, $E_p = \sqrt{M^2+p^2}$, $\bar{\nu} = \sqrt{M^2+p^2+q^2+2pqcos\alpha} \ - \ E_p$, $\bar{Q}^2 = |\vec{q}|^2 - \bar{\nu}^2$ and $\bar{\tau} = \bar{Q}^2/4M^2$.

In Eqs. (8) - (11) the integration limits and $cos\alpha$ are determined, as usual, by energy conservation [19].

3. The three-body ground-state in the hyperspherical-harmonic method and the spin-dependent spectral function

The spin-dependent spectral functions of ^{3}He and ^{3}H, Eqs.(5) and (6), have been calculated from three-body wave functions obtained using the PHH expansion. This technique represents a very efficient and accurate method for describing the system, and explicitely includes pair correlation functions in order to take into account the short range repulsion of the nucleon-nucleon (NN) interaction. In the following the main features of the method [14] will be briefly recalled.

The three-nucleon wave function with total angular momentum $J\mathcal{M}$ and total isospin TT_z can be written, in the LS coupling scheme, as

$$\psi^{TT_z}_{J\mathcal{M}} = \sum_{i=1,3} \left\{ \sum_{\alpha=1}^{N_c} \Phi_\alpha(x_i, y_i) \mathcal{Y}_\alpha(jk, i) \right\} \tag{12}$$

with

$$\mathcal{Y}_\alpha(jk, i) = \left\{ [Y_{\ell_\alpha}(\hat{x}_i) Y_{L_\alpha}(\hat{y}_i)]_{\Lambda_\alpha} [s^{jk}_\alpha s^i_\alpha]_{S_\alpha} \right\}_{J\mathcal{M}} [t^{jk}_\alpha t^i_\alpha]_{TT_z} \tag{13}$$

where x_i, y_i are the moduli of the Jacobi coordinates, α runs over the three–body channels included in the partial wave decomposition of the wave function and (jk, i) are cyclic permutations of $(12, 3)$. The total number of channels considered is N_c. The two–dimensional amplitudes $\Phi_\alpha(x_i, y_i)$ are expanded in terms of the PHH basis

$$\Phi_\alpha(x_i, y_i) = \rho^{\ell_\alpha + L_\alpha} f_\alpha(x_i) \Big[\sum_{K=K_0}^{K_\alpha} u^\alpha_K(\rho) \ {}^{(2)}P^{\ell_\alpha + L_\alpha}_K(\phi_i) \Big] \tag{14}$$

where $x_i = \rho \cos(\phi_i)$ and $y_i = \rho \sin(\phi_i)$ are the hyperspherical variables, $K_0 = \ell_\alpha + L_\alpha$ and ${}^{(2)}P^{\ell_\alpha + L_\alpha}_K(\phi_i)$ is an hyperspherical polynomial [20]. The pair correlation functions $f_\alpha(x_i)$ are introduced in order to accelerate the convergence of the expansion and are determined by the NN potential as explained in [14]. The unknown quantities in Eq.(14) are the hyperradial functions $u^\alpha_K(\rho)$, which are obtained through the Rayleigh-Ritz variational principle.

Convergence and accuracy reached by increasing the number of terms in the expansions (12) and (14) are discussed in [14] for realistic NN potentials with and without three-nucleon interaction (TNI) terms included in the Hamiltonian of the system. Typically with $N_c = 18$ and about 80 hyperradial functions an accuracy of the order of a few keV is obtained for the binding energy of the system. In the calculations of the spin-dependent spectral function we have used three-body wave functions corresponding to a variety of NN potentials and TNI's. In particular we have considered: i) NN interactions such as the Argonne Av14 interaction [21] and the Reid soft-core [22] RSCv8 potential (that represents the local version of the original one with eight operators only), and ii) the Brazil three-body force [23] (BR) and the Tucson-Melbourne one [24] (TM). When the TNI have been taken into account, the cut-off parameter was adjusted in order to give the triton experimental binding energy $B(^3H) = 8.48$ MeV. It should be emphasyzed that for the ^{3}He ground-state the Coulomb interaction between the two protons has been included, and this possibility represents a typical feature of the variational approaches. In Table I, binding energies and probabilities of symmetric-S, S', D, and P components of ^{3}H and ^{3}He wave functions, corresponding to the interactions we have adopted, are listed. The interactions we considered have sizable differences in their structures (e.g. the RSCv8 interaction has a Yukawa-type repulsion at short distances, whereas the Av14 interaction remains finite), and these differences are reflected in the corresponding three-body wave functions. In particular the percentages of the small components are affected by the choice of the potential, as illustrated, e.g., by $P_{S'}$ that varies up to 30% by changing from RSCv8 interaction to Av14 interaction + three-body forces.

Table I: Binding energies and probabilities of symmetric-S, S', D and P waves for ^{3}H and ^{3}He obtained with different ISI (see text for the legend).

^{3}H					
ISI	B(MeV)	$P_S(\%)$	$P_{S'}(\%)$	$P_D(\%)$	$P_P(\%)$
Av14	7.683	89.831	1.126	8.967	0.076
RSCv8	7.600	88.920	1.342	9.654	0.084
Av14 + BR	8.485	89.388	0.928	9.544	0.140
Av14 + TM	8.485	89.645	0.933	9.261	0.161
^{3}He					
ISI	B(MeV)	$P_S(\%)$	$P_{S'}(\%)$	$P_D(\%)$	$P_P(\%)$
Av14	7.032	89.680	1.314	8.931	0.075
RSCv8	6.958	88.757	1.550	9.610	0.083
Av14 + BR	7.809	89.276	1.077	9.509	0.138
Av14 + TM	7.809	89.526	1.083	9.233	0.158

In order to calculate ${}_N\langle \vec{p},\sigma;\psi_{f_{(A-1)}}|\psi^{T,T_z}_{J,\mu}\rangle$, see Eq.(5), we Fourier-transformed the following overlap

$$G^{T_z,\mu}_{f,\sigma,\tau}(\vec{y}) = \langle \chi^{1/2}_\sigma\ \xi^{1/2}_\tau \vec{y};\psi_f|\psi^{1/2,T_z}_{1/2,\mu}\rangle =$$
$$= \langle \frac{1}{2}\tau T_{12}\tau_{12}|\frac{1}{2}T_z\rangle \sum_{\ell\ m\ j\ m_j} \langle J_{12}m_{12}\frac{1}{2}\sigma|jm_j\rangle\langle \ell m j m_j|\frac{1}{2}\mu\rangle\ g^f_{\ell j}(y)\ Y_{\ell m}(\hat{y}) \qquad (15)$$

where $f \equiv [J_{12},\ m_{12},\ S_{12},\ T_{12},\ \tau_{12},\ \lambda,\ E_{12}]$ (cf. [25]) represents the quantum numbers of the two-body wave function $|\psi_f(\vec{x})\rangle$, corresponding to the particles (1,2) that interact with the same potential as in the three-body hamiltonian; $\chi^{1/2}_\sigma$ and $\xi^{1/2}_\tau$ are the spin and isospin functions of the third particle. The functions $g^f_{\ell j}(y)$ are the overlaps between the three-body ground-state and the two-body wave function coupled to the third particle spin, isospin, and orbital momentum eigenfunctions. Once the functions $G^{T_z,\mu}_{f,\sigma,\tau}$ have been obtained, the evaluation of the functions $B^N_{0(1,2),\mathcal{M}}$ is performed following the expressions of Ref.[8].

Before presenting the actual results of these functions for the case of ^{3}He, it is interesting to consider the effective polarization of the nucleon, $\mathcal{P}^N$, Eq.(7), that represents an integral property of the three-body wave function. In Table II the values of $\mathcal{P}^N$ for ^{3}He are listed for the different interactions we have used (the corresponding values for ^{3}H can be obtained by isospin symmetry once the Coulomb interaction is disregarded). In particular, for the sake of completeness, we have also reported the effective polarization corresponding to the case when the Coulomb interaction is switched off in ^{3}He. As pointed out in [16] the differences between $\mathcal{P}^N$ values can be traced back to the differences in the probabilities of S' and D waves (see Table I). It is worth noting that Coulomb potential and TNI effects are small and become important, in percentage, for the proton effective polarization, since this

Table II.: The values of the nucleon effective polarization in ^{3}He, obtained with different ISI (see text for the legend).

ISI	$\mathcal{P}_n$ %	$\mathcal{P}_p$ %
Av14	87.37	-2.57
Av14+Cou	87.30	-2.49
Av14+Cou+BR	86.65	-2.77
Av14+Cou+TM	87.01	-2.68
RSCv8	86.12	-2.67
RSCv8+Cou	86.19	-2.76

quantity is small by itself.

In Figs. 1 and 2, the unpolarized spectral function $B^{p(n)}_{0,\frac{1}{2}}(|\vec{p}|,E)$ and the functions $|B^{p(n)}_{1,\frac{1}{2}}(|\vec{p}|,E)|$ and $|B^{p(n)}_{2,\frac{1}{2}}(|\vec{p}|,E)|$ obtained from the ^{3}He wave function corresponding to the Av14 potential model *plus* the Coulomb interaction, are shown (in the case of the proton the curve corresponding to a spectator deuteron is not presented). It has to be pointed out that the introduction of three-body forces does not change sizably the overall behaviour, and produces only small differences in the values for any given (E,p); these differences could be important in the calculation of tiny effects, such as the cross section of exclusive reactions where the proton is detected, since large cancellations between contributions produced by a spectator pair in the deuteron state and in the continuum occur. The spin-dependent spectral function was already calculated, without Coulomb interaction: i) in Ref. [8], adopting a variational three-body wave function corresponding to the Reid soft-core interaction [22]; and ii) in Ref.[9], using a Faddeev wave function and the Paris potential [26]. The comparison between our results of Figs. 1 and 2, obtained without three-body forces but with the Coulomb interaction, and the corresponding ones of [8], obtained with a different two-body nuclear force and no Coulomb interaction, illustrates the sensitivity to the choice of the two-body part of the interaction, showing that the gross features remain unchanged. Relevant changes can be found only in $|B^{p(n)}_{1,\frac{1}{2}}(|\vec{p}|,E)|$ and $|B^{p(n)}_{2,\frac{1}{2}}(|\vec{p}|,E)|$ (cf. also Table II). Moreover, a smoother behaviour is observed in the present spectral functions, due to the improved accuracy in the description of the bound-state wave functions.

4. The em polarized responses in ^{3}He and ^{3}H

The nuclear responses, for both ^{3}He and ^{3}H, have been obtained by using the spin-dependent spectral functions calculated from the variational wave functions described in Sect. 3. The results corresponding to CC1 and CC2 prescriptions for the off-energy-shell em nucleon tensor are essentially the same for $R_{TL'}$, while, in the whole range $0.1 \leq Q^2 \leq 2(GeV/c)^2$ we have investigated, the differences for the proton and neutron contributions to $R_{T'}$ are in general less than 2%, except a 3% variation for the negligible neutron contribution

in ^{3}H. Therefore in the following we report only the results obtained by the prescription CC1, i.e. by using Eqs. (8)-(11).

Before analyzing in detail the em polarized responses, let us compare our predictions for the asymmetry of ^{3}He, defined by

$$A = \frac{\Delta}{\Sigma} \tag{16}$$

(cf. Eqs. (2) and (3)), with the most recent data from inclusive experiments that should be proportional, at qe peak, to $R^{^3He}_{T'}$ [5] and $R^{^3He}_{TL'}$ [6]. In Figs. 3 and 4, the results obtained by using different ISI are shown. In particular, in Figs. 3(a) and 4(a) the theoretical predictions corresponding to: i) Av14 potential + Coulomb interaction, ii) RSCv8 potential + Coulomb interaction and iii) Paris potential without Coulomb interaction, from [9], are compared with the experimental data; it is worth noting that for the kinematics of Ref. [5], where $A_{peak} \propto R^{^3He}_{T'}$, the asymmetry does not appreciably change by varying the two-body ISI (less than 2% at the qe peak), while for the kinematics of Ref. [6], where $A_{peak} \propto R^{^3He}_{TL'}$, there is a little bit higher variation (less than 4% at the qe peak), in line with the findings of the theoretical analysis contained in [6]. In particular for the latter kinematics, the differences among the theoretical curves are smaller than the ones found in [6], where the original RSC interaction without Coulomb potential was considered. Differences are even smaller if we consider the effects of three-body forces, as shown in Figs. 3(b) and 4(b). These results are quite reasonable in view of the tiny ISI effects on the effective polarizations shown in Table II. One can conclude that at least for low values of momentum transfer ($Q^2 \leq 0.2$ $(GeV/c)^2$), changes in the asymmetry due to ISI are small at the qe peak and therefore the model dependence seems to be under control, since it amounts to 3-4%, at most. In Figs. 3 and 4 the neutron contribution to the total responses is shown separately. From a comparison between such a contribution and the total responses one can see that the presence of the proton, in particular for $R^{^3He}_{TL'}$, represents the major obstacle in the extraction of neutron em form factors, as already pointed out in [6, 8, 9].

In what follows we will carry out a systematic investigation of the model dependence, due to ISI and proton contribution, in the extraction of neutron form factors for Q^2 up to 2 $(GeV/c)^2$, i.e. for a kinematical region relevant for TJNAF. Moreover, we will show the corresponding results for ^{3}H in order to gain some insight on the possibility to reduce the model dependence by taking advantage of the isospin symmetry, partially broken by the Coulomb interaction.

The analysis of the polarized responses at qe peak is motivated by the expectation of a clear disentangling of the nuclear structure from the nucleon form factors. For ^{3}He and ^{3}H, even if the FSI are present, Eqs. (10) and (11) can be written as follows

$$R^{^3He}_{T'}\left(Q^2,\nu\right) = \frac{Q^2}{2qM}\left[2\ \left(G^p_M\left(Q^2\right)\right)^2 \mathcal{H}^p_{T'}\left(Q^2,\nu\right) + \left(G^n_M\left(Q^2\right)\right)^2 \mathcal{H}^n_{T'}\left(Q^2,\nu\right)\right] \tag{17}$$

$$R^{^3He}_{TL'}\left(Q^2,\nu\right) = -\sqrt{2}\left[2\ G^p_E\left(Q^2\right) G^p_M\left(Q^2\right) \mathcal{H}^p_{TL'}\left(Q^2,\nu\right) + G^n_E\left(Q^2\right) G^n_M\left(Q^2\right) \mathcal{H}^n_{TL'}\left(Q^2,\nu\right)\right] \tag{18}$$

$$R^{^3H}_{T'}\left(Q^2,\nu\right)=\frac{Q^2}{2qM}\left[\left(G^p_M\left(Q^2\right)\right)^2\mathcal{T}^p_{T'}\left(Q^2,\nu\right)+2\ \left(G^n_M\left(Q^2\right)\right)^2\mathcal{T}^n_{T'}\left(Q^2,\nu\right)\right] \tag{19}$$

$$R^{^3H}_{TL'}\left(Q^2,\nu\right)=-\sqrt{2}\left[G^p_E\left(Q^2\right)G^p_M\left(Q^2\right)\mathcal{T}^p_{TL'}\left(Q^2,\nu\right)+2\ G^n_E\left(Q^2\right)G^n_M\left(Q^2\right)\mathcal{T}^n_{TL'}\left(Q^2,\nu\right)\right] \tag{20}$$

where the Sachs form factors, $G^N_M=F^N_1+F^N_2$ and $G^N_E=F^N_1-F^N_2\frac{Q^2}{4M^2}$, have been introduced. The functions $\mathcal{H}^N_{T'(TL')}$ and $\mathcal{T}^N_{T'(TL')}$ in general contain both the nuclear structure, which within PWIA is described by $B_{0,1,2}$, and ratios of nucleon form factors, and are defined by

$$\begin{aligned}\mathcal{H}^{p(n)}_{T'(TL')}\left(Q^2,\nu\right)&=\frac{R^{^3He,p(n)}_{T'(TL')}\left(Q^2,\nu\right)}{K^{p(n)}_{T'(TL')}\left(Q^2\right)}\\ \mathcal{T}^{p(n)}_{T'(TL')}\left(Q^2,\nu\right)&=\frac{R^{^3H,p(n)}_{T'(TL')}\left(Q^2,\nu\right)}{K^{p(n)}_{T'(TL')}\left(Q^2\right)}\end{aligned} \tag{21}$$

with $R^{^3He,p(n)}_{T'(TL')}$ and $R^{^3H,p(n)}_{T'(TL')}$ the proton (neutron) contribution to the total responses, $K^{p(n)}_{T'}=Q^2\mathcal{N}^{p(n)}(G^{p(n)}_M)^2/2qM$ and $K^{p(n)}_{TL'}=-\sqrt{2}\mathcal{N}^{p(n)}G^{p(n)}_EG^{p(n)}_M$. It should be stressed that the usefulness of Eqs. (17) and (18) in the extraction of G^n_E and G^n_M is related to the possibility that $\mathcal{H}^N_{T'(TL')}$ be independent of nucleon form factors, at least at qe peak. Within PWIA, actually, the functions $\mathcal{H}^N_{T'(TL')}$ and $\mathcal{T}^N_{T'(TL')}$ become independent of nucleon form factors at the qe peak, and even almost independent of Q^2. The first feature can be immediately seen, since at qe peak $p\approx 0$, $E_p\approx M$ and $\bar{\nu}=Q^2/2M$; thus retaining only p-leading terms in Eqs. (10) and (11) one has for ^{3}He,

$$\begin{aligned}&\mathcal{H}^N_{T'}\left(Q^2,\nu_{peak}\right)\approx\mathcal{F}^{^3He,N}_{T'}\left(Q^2,\nu_{peak}\right)=\\ &=2\pi\int\limits_{E_{min}}^{E_{max}(Q^2,\nu_{peak})}dE\int\limits_{p_{min}(Q^2,\nu_{peak},E)}^{p_{max}(Q^2,\nu_{peak},E)}p\ dp\ \left(B^N_1(p,E)\ +B^N_2(p,E)\,cos^2\alpha\right)\end{aligned} \tag{22}$$

$$\begin{aligned}&\mathcal{H}^N_{TL'}\left(Q^2,\nu_{peak}\right)\approx\mathcal{F}^{^3He,N}_{TL'}\left(Q^2,\nu_{peak}\right)=\\ &=2\pi\int\limits_{E_{min}}^{E_{max}(Q^2,\nu_{peak})}dE\int\limits_{p_{min}(Q^2,\nu_{peak},E)}^{p_{max}(Q^2,\nu_{peak},E)}p\ dp\ \left(B^N_1(p,E)\ +\frac{B^N_2(p,E)}{2}sin^2\alpha\right)\end{aligned} \tag{23}$$

For ^{3}H the same approximations hold, but the structure functions $B_{0,1,2}$, entering the analogous equations, are the appropriate ones for such a nucleus, i.e. they are obtained without Coulomb interaction and exchanging the proton with the neutron.

In Fig. 5, i) the functions $\mathcal{H}^N_{T'(TL')}(Q^2,\nu_{peak})$ and $\mathcal{T}^N_{T'(TL')}(Q^2,\nu_{peak})$ calculated by using the full PWIA expressions (cf. Eqs.(10), (11) and (21)) and the Galster nucleon form factors [27]; and ii) their approximations $\mathcal{F}^{\ni\mathcal{H}],\mathcal{N}}_{\mathcal{T}'(\mathcal{TL}')}\left(\mathcal{Q}^{\in},\nu_{\surd^{]\dashv\|}}\right)$ and $\mathcal{F}^{\ni\mathcal{H},\mathcal{N}}_{\mathcal{T}'(\mathcal{TL}')}\left(\mathcal{Q}^{\in},\nu_{\surd^{]\dashv\|}}\right)$ (see Eqs.(22) and (23)) are shown. Since the approximations are quite good, this indicates that, within PWIA, the functions $\mathcal{H}^N_{T'(TL')}(Q^2,\nu_{peak})$ and $\mathcal{T}^N_{T'(TL')}(Q^2,\nu_{peak})$ become independent of the nucleon form factors, namely the factorization of the latter quantities out of the nuclear structure is confirmed at a large extent. Therefore, the expectation of extracting information on the neutron properties from polarized ^{3}He is strengthened (cf. [2], where only the spin-dependent momentum distribution was considered). It should be pointed out that using different nucleon form factors, such as the Gari-Krumpelmann [28] or the Hoehler [29] ones, the factorization is even better. Moreover, the nuclear structure functions, $\mathcal{H}^N_{T'(TL')}(Q^2,\nu_{peak})$ and $\mathcal{T}^N_{T'(TL')}(Q^2,\nu_{peak})$, have a constant behaviour over a wide range of Q^2 and this striking feature can be of great help in disentangling nucleon form factors from the nuclear structure, as shown in Sect. 5. Finally, if we disregard the effects of the Coulomb force (an effect of the order of a few percent for the neutron in ^{3}He) the functions $\mathcal{T}^p_{T'(TL')}(Q^2,\nu_{peak})$ measured in ^{3}H, represent a very good approximations for $\mathcal{H}^n_{T'(TL')}(Q^2,\nu_{peak})$.

In what follows, after a general analysis of the responses, we will sketch a possible way for minimizing the model dependence just exploiting the above mentioned features of the polarized responses.

In Figs. 6(a,b) and 7(a,b) our PWIA results of $R_{T'}$ and $R_{TL'}$ for ^{3}He and ^{3}H are shown through the ratios $R_{T'}/G_D^2$ and $R_{TL'}/G_D^2$ ($G_D = 1/(1+Q^2/0.71)^2$), at qe peak and for Q^2 up to 2 $(GeV/c)^2$. The variations due to the different choices of two- and three-body nuclear forces or to the presence of the Coulomb interaction remain less than 5-6% over the whole range of Q^2 explored. It turns out that for ^{3}He the effects due to Coulomb potential and TNI are larger, in percentage, in the proton contribution than in the neutron one (cf. also the values of the effective polarization listed in Table II, where the same behaviour can be found). The Coulomb potential negligibly affects $R^{^3He}_{T'}$, since it yields a different sign effect in the proton and neutron contributions.

In view of the analysis we have carried out, Figs. 6(c) and 7(c) are of particular interest, since they illustrate the relevance of the proton contribution in ^{3}He and the tiny effect of the neutron in ^{3}H. We can see that while the neutron can be safely disregarded in ^{3}H (the relative contribution is less than 3 %), this fact does not occur for the proton in ^{3}He. In the kinematical interval we have considered, for $R^{^3He}_{TL'}$ the relative proton contribution ranges between 80%, at low values of Q^2, and 40%, at the highest ones. For $R^{^3He}_{T'}$ the proton contribution is not as dramatic as in the case of $R^{^3He}_{TL'}$. As a consequence of this limited effect $R^{^3He}_{T'}$ and $R^{^3H}_{T'}$ are nearly proportional, i.e. $R^{^3He}_{T'} \approx (\mu_n/\mu_p)^2 R^{^3H}_{T'}$, cf. Figs. 6(a) and 7(a); the experimental evidence of this proportionality could be an indication of the smallness of the proton contribution. However, even for $R^{^3He}_{T'}$ this contribution is not negligible ($\approx$ 10%) and has a value about twice larger than the uncertainties due to ISI. The conclusions that can be drawn from Figs. 6 and 7 are in order: i) the neutron in ^{3}H can be safely disregarded at a level of a few percent; thus a measurement of $R^{^3H}_{T'(TL')}$ allows

to check PWIA predictions such as factorizable responses, an almost constant behaviour of $\mathcal{T}^N_{T'}(Q^2,\nu_{peak})$ and $\mathcal{T}^N_{TL'}(Q^2,\nu_{peak})$, and their equality; ii) if the small Coulomb effects are disregarded, one can apply the isospin symmetry in order to identify $\mathcal{H}^n_{T'(TL')}$ with $\mathcal{T}^p_{T'(TL')}$, obtained from measurements of ^{3}H responses, and in this way one could reduce the model dependence in the extraction of neutron form factors; iii) the proton contribution in ^{3}He cannot be neglected, even at high Q^2. As a final remark, let us note that an experimental observation of a constant behaviour of $\mathcal{T}^p_{T'(TL')}(Q^2,\nu_{peak})$ could give relevant information both on the approximation of the nucleon form factors in the three-nucleon system as the free ones and on the prescriptions for the off-energy-shell em nucleon current.

In the following Section we will illustrate how to minimize the model dependence related to the above mentioned proton contribution.

5. The extraction of G^n_E and G^n_M

The almost constant behaviour of the proton structure function $\mathcal{H}^p_{TL'}(Q^2,\nu_{peak})$, shown in Fig. 5(b), suggests a possible way for extracting information on the proton contribution to $R^{^3He}_{TL'}(Q^2,\nu_{peak})$. As a matter of fact if we divide the *total response* $R^{^3He}_{TL'}(Q^2,\nu_{peak})$ by the proton form factors, assumed well-known, or better by $K^p_{TL'}(Q^2) = -2\sqrt{2}\ G^p_M G^p_E$, we obtain, within PWIA, an almost constant term ($\mathcal{H}^p_{TL'}$) *plus* a Q^2-dependent one, i.e. (see Eq.(18))

$$\frac{R^{^3He}_{TL'}(Q^2,\nu_{peak})}{K^p_{TL'}(Q^2,\nu_{peak})} = \mathcal{H}^p_{TL'}\left(Q^2,\nu_{peak}\right) + \frac{G^n_E(Q^2)\,G^n_M(Q^2)}{2G^p_E(Q^2)\,G^p_M(Q^2)}\mathcal{H}^n_{TL'}\left(Q^2,\nu_{peak}\right)\ medskip \quad (24)$$

For small values of the momentum transfer, the Q^2-dependent term should be linear in Q^2, due to the presence of the neutron charge form factor, G^n_E, and the almost constant behaviour of the neutron structure function $\mathcal{H}^n_{TL'}(Q^2,\nu_{peak})$; therefore Eq.(24) becomes

$$\frac{R^{^3He}_{TL'}(Q^2,\nu_{peak})}{K^p_{TL'}(Q^2,\nu_{peak})} \approx \tilde{\mathcal{H}}^p_{TL'} + \alpha\ Q^2 \quad (25)$$

where $\tilde{\mathcal{H}}^p_{TL'}$ is a constant value. This behaviour is confirmed by the direct calculations presented in Fig. 8, where the ratio $R^{^3He}_{TL'}(Q^2,\nu_{peak})/K^p_{TL'}(Q^2)$, evaluated within PWIA, is plotted for $0.1 \leq Q^2 \leq 0.3\ (GeV/c)^2$. This range of momentum transfer can be easily understood, since at very low values of Q^2 the response vanishes, and therefore we have to move from this particular region, while at high values of momentum transfer G^n_E/G^p_E is no more linear in Q^2 (see, e.g. the parametrizations of [27, 29]).

The extraction of the proton contribution to $R^{^3He}_{TL'}(Q^2,\nu_{peak})$ should proceed as follows: after measuring $R^{^3He}_{TL'}(Q^2,\nu_{peak})$ in the proposed range, one should check whether the data exhibit the linear behaviour shown in Fig. 8, and in the positive case one can determine $\tilde{\mathcal{H}}^p_{TL'}$, to be compared with theoretical predictions. From the experimental value of $\tilde{\mathcal{H}}^p_{TL'}$, one obtains $R^{^3He,p}_{TL'}(Q^2,\nu_{peak})$ over the whole range of Q^2, and singles out the neutron contribution $R^{^3He,n}_{TL'}(Q^2,\nu_{peak})$, which is sensitive to the neutron charge form factor. It should be pointed

out that the results shown in Fig. 8 rely on the factorization of the response, as discussed in Sect. 4, and on the absence of effects such as FSI; therefore whether the linear behavior predicted by the PWIA (cf. Eq.(25)) is not observed, essential information on both the reaction mechanism and the presence of other effects can be extracted. For instance, a linear behaviour in Q, and not in Q^2, would mean that the variation of $R^{^3He}_{TL'}(Q^2, \nu_{peak})$ is dominated by $R^{^3He,p}_{TL'}$, since the Q^2-dependence of the neutron part in $R^{^3He}_{TL'}$ is always governed by G^n_E. In this case we can compare the theoretical calculations of the proton contribution, that are not affected by unknown form factors, with the experimental data, obtaining constraints on $R^{^3He,p}_{TL'}$. Therefore, in any case, either PWIA holds or not, the measurement of $R^{^3He}_{TL'}(Q^2, \nu_{peak})$ at low Q^2 will yield valuable information on the proton, to be used in further steps.

Once we have an experimental estimate of the proton contribution to the transverse-longitudinal response, $R^{^3He,p}_{TL'}(Q^2, \nu_{peak})$, we could achieve an estimate of proton contribution to the transverse response, $R^{^3He,p}_{T'}(Q^2, \nu_{peak})$, by using the β-kinematics analyzed in [8]. The choice of the polarization angle β, with $cos\beta = \vec{S}_A \cdot \vec{k}_1/|\vec{k}_1|$ is suggested by: i) the direct connection with the experimental set-up and ii) more important, the low dependence of β_{critic} (see below) upon kinematical conditions. It turns out that the proton contribution to the polarized cross section, $\Delta^p(Q^2, \nu_{peak})$, (cf. Eq. (3)) vanishes when the polarization angle θ^*, reaches a critical value or, see Eq.(4), when the polarization angle β reaches β_{critic}. An estimate of such an angle, at the qe peak, can be obtained by measuring the protons knocked out along the direction of $\vec{q}$, since at the qe peak protons should be emitted preferably along such a direction. It is worth noting that an exclusive measurement of protons is much easier than the one of neutrons, and moreover row data are sufficient for estimating β_{critic}, since one has only to determine the polarization angle where the polarized response $\Delta^p(Q^2, \nu_{peak})$ changes sign. After determining β_{critic} at the qe peak, one can obtain the corresponding θ^*, see Eq.(4), and finally $R^{^3He,p}_{T'}(Q^2, \nu_{peak})/R^{^3He,p}_{TL'}(Q^2, \nu_{peak})$ from the equation $\Delta^p(Q^2, \nu_{peak}) = 0$, see Eq.(3). It should be pointed out that the measurement of β_{critic} is related to a ratio of response functions, and therefore, even in presence of other effects, the PWIA prediction should represent a good approximation; furthermore, it turns out that β_{critic} does not sizably vary as function of Q^2 (at most a few percent), while θ^*_{critic} does. In Fig. 9, the angle β_{critic} is shown for different ISI, at a scattering angle $\theta_e = 50^o$. It should be pointed out that an error of $\pm 1^o$ on the measurement of β_{critic} produces an uncertainty of the order 5% on the ratio $R^{^3He,p}_{T'}/R^{^3He,p}_{TL'}$ while an error of $\pm 2^o$ produces an uncertainty of the order 12%. Even a large uncertainty on $R^{^3He,p}_{T'}$ does not prevent the extraction of the neutron magnetic form factor, since $R^{^3He,p}_{T'}$ is small, of the order of 10% of the total response, as shown in Fig.6(c).

In conclusion, through an estimate of $R^{^3He,p}_{TL'}$, from the low Q^2 behaviour of the total response $R^{^3He}_{TL'}$, and an estimate of $R^{^3He,p}_{T'}$, from β_{critic}, one can obtain the neutron contribution to the total responses $R^{^3He}_{TL'}$ and $R^{^3He}_{T'}$, respectively. From the ratio $R^{^3He,n}_{TL'}/R^{^3He,n}_{T'}$ one can obtain the ratio G^n_E/G^n_M, assuming that the functions $\mathcal{H}^n_{TL'}$ and $\mathcal{H}^n_{T'}$ are equal, as in the case of PWIA; moreover, introducing a theoretical prediction for $\mathcal{H}^n_{T'(TL')}$ one could extract G^n_E and G^n_M separately.

Finally a measurement of the polarized ^{3}H could give the possibility of an almost model-independent extraction of both the neutron form factors, since the structure functions $\mathcal{H}^n_{TL'}$ and $\mathcal{H}^n_{T'}$ could be estimated through $\mathcal{T}^p_{TL'}$ and $\mathcal{T}^p_{T'}$, disregarding the Coulomb effects.

6. Conclusion

In this paper we have presented the results of our investigation on the em inclusive responses of polarized ^{3}He and ^{3}H, within the PWIA. We have calculated the spin-dependent spectral functions [8] of the three-nucleon system, from bound-state wave functions, obtained using the pair correlated hyperspherical-harmonic expansion [14]. Different realistic two- and three-body nuclear forces, such as i) the Argonne v14 potential and the RSCv8 one, and ii) the Brazil and Tucson-Melbourne three-nucleon interactions, have been considered; moreover, the Coulomb interaction has been taken into account in the case of ^{3}He. Then we have evaluated the transverse-longitudinal polarized response and the transverse one, focusing at the qe peak, for Q^2 up to 2 $(GeV/c)^2$. The detailed analysis of the Q^2-behaviour of the inclusive responses has allowed: i) to investigate the model dependence upon the initial state interaction and ii) to suggest possible experiments for determining the proton contribution to $R^{^3He}_{TL'}(Q^2,\nu_{peak})$ and $R^{^3He}_{T'}(Q^2,\nu_{peak})$, which represents one of the major obstacle in the experimental extraction of the neutron form factors. The model dependence upon two- and three-nucleon interactions and Coulomb potential as well, amounts to a few percent; for ^{3}He the Coulomb and TNI effects are more relevant for the proton contribution than the neutron one, as in the case of the effective polarization.

The presence of the proton affects quite differently the polarized responses, since in $R^{^3He}_{T'}(Q^2,\nu_{peak})$ it is $\approx$ 10 %, while in $R^{^3He}_{TL'}(Q^2,\nu_{peak})$ it ranges between 80%, at low values of Q^2, and 40%, at the highest ones. This proton predominance can be turned in our advantage, since PWIA predicts a linear behaviour in Q^2 for the ratio $R^{^3He}_{TL'}(Q^2,\nu_{peak}) \,/\, \left(-2\sqrt{2}\, G^p_M(Q^2)\, G^p_E(Q^2)\right)$ at low momentum transfer, $0.1 \leq Q^2 \leq 0.3$ $(GeV/c)^2$. Therefore a comparison with the experimental data can yield $R^{^3He,p}_{TL'}$ or, at least, definite information on the proton contribution, e.g. on the presence of factorization and/or FSI.

The proton contribution to $R^{^3He}_{T'}$ can be measured from the ratio $R^{^3He,p}_{T'}(Q^2,\nu_{peak}) \,/\, R^{^3He,p}_{TL'}(Q^2,\nu_{peak})$ obtained through an accurate determination of the polarization angle β_{critic}, where the proton contribution to the polarized cross section, see Eq.(3), is vanishing. The PWIA prediction of this angle could be used as a reliable guideline for the experimental measurements, since β_{critic} depends upon the ratio of responses, possibly less sensitive to various effects, such as FSI, than each response separately.

The proposed measurements could allow the extraction of the neutron contribution to the total responses and therefore an estimate of the ratio G^n_E/G^n_M. If one introduces theoretical calculations of the nuclear structure functions $\mathcal{H}^n_{T'(TL')}$, one could even obtain G^n_E and G^n_M separately. Finally, it should be pointed out that a measurement of the em inclusive responses of polarized ^{3}H could give the possibility to check more directly the reaction mechanism, namely the factorization at the qe peak (essential for extracting the neutron form factors), and to obtain the nuclear structure functions, $\mathcal{T}^p_{T'(TL')}$. In this case,

one can substantially lower the model dependence in the extraction of G_E^n and G_M^n by using the ^{3}H structure functions as an experimental estimate of the corresponding quantities for ^{3}He.

Calculations for taking into account FSI are in progress.

6. Acknowledgment

The authors are very grateful to C. Ciofi degli Atti and S. Rosati for the encouragement in carrying on this work and for valuable discussions. Two of us (E.P. and G.S.) also acknowledge stimulating discussions with H. Gao and O. Hansen.

References

[1] S. Platchkov et al., *Nucl. Phys.* **A 510**, 740 (1990).

[2] B. Blankleider and R. M. Woloshyn, *Phys. Rev.* **C 29**, 538 (1984).

[3] a) C. E. Jones-Woodward et al., *Phys. Rev.* **C 47**, 110 (1993) ; b) C. E. Jones-Woodward et al., *Phys. Rev.* **C 52**, 1520 (1995).

[4] A. K. Thompson et al., *Phys. Rev. Lett.* **68**, 2901 (1992).

[5] H. Gao et al., *Phys. Rev.* **C 50**, R546 (1994).

[6] J. O. Hansen et al., *Phys. Rev. Lett.* **74**, 654 (1995).

[7] H. Gao et al., E-95-001 CEBAF approved experiment.

[8] C. Ciofi degli Atti, E. Pace and G. Salmè, *Phys. Rev.* **C 46**, R1591 (1992); Phys. Rev. **C 51**, 1108 (1995).

[9] R. W. Schültze and P.U. Sauer, *Phys. Rev.* **C 48**, 38 (1993).

[10] J. Golack, H. Witala, H. Kamada, D. Hüber, S. Hishikawa and W. Glöckle, *Phys. Rev.* **C 52**, 1216 (1995).

[11] S. Martinelli, H. Kamada, G. Orlandini and W. Glöckle, *Phys. Rev.* **C 52**, 1778 (1995).

[12] O. Benhar, E. Pace and G. Salmè, *Phys. Lett.* **B195**, 13 (1987).

[13] H. Meier-Hajduk, U. Oelfke and P.U. Sauer, *Nucl. Phys.* **A499**, 637 (1989).

[14] A. Kievsky, M. Viviani and S. Rosati, *Nucl. Phys.* **A551**, 241 (1993); **A577**, 511 (1994).

[15] T. W. Donnelly and A. S. Raskin, *Ann. Phys. (N.Y.)* **169**, 247 (1986).

[16] J. L. Friar, B.F. Gibson, G.L. Payne, A.M. Bernstein and T.E. Chupp, *Phys. Rev.* **C 42**, 2310 (1990).

[17] T. De Forest, Jr., *Nucl. Phys.* **A392**, 232 (1983).

[18] S. Pollock, H.W.L. Naus, J.H. Kock, *Phys. Rev.* **C 53**, 2304 (1996).

[19] C. Ciofi degli Atti, E. Pace and G. Salmè, *Phys. Rev.* **C 43**, 1155 (1991).

[20] M. Fabre de la Ripelle, *Ann. Phys. (N.Y.)* **147**, 281 (1983).

[21] R. B. Wiringa, R. A. Smith and T. A. Ainsworth, *Phys. Rev.* **C 29**, 1207 (1984).

[22] R. V. Reid, *Ann. Phys. (N.Y.)* **50**, 411 (1968).

[23] H. T. Coelho, T. K. Das and M. R. Robilotta, *Phys. Rev.* **C 28**, 1812 (1983).

[24] S. A. Coon, M.D. Scadron, P.C. McNamee, B.R. Barret, D.W.E. Blatt and B.H.J. McKellar, *Nucl. Phys.* **A317**, 242 (1979); S. A. Coon and W. Glökle, *Phys. Rev.* **C 23**, 1790 (1981).

[25] C. Ciofi degli Atti, E. Pace and G. Salmè, *Phys. Lett.* **B141**, 14 (1984).

[26] M. Lacombe, B. Loiseau, S.M. Richard, R. Vinh Mau, J. Cotè, P. Pirès and R. de Tourreil, *Phys. Rev.* **C21**, 861 (1980).

[27] S. Galster et al., *Nucl. Phys.* **B32**, 221 (1971).

[28] M. Gari and W. Krumpelmann, *Z. Phys.* **A322**, 689 (1985); *Phys. Lett.* **B 173**, 10 (1986).

[29] G. Hoehler et al., *Nucl. Phys.* **B 114**, 505 (1976).

FIGURE CAPTIONS

Fig. 1(a). The proton unpolarized spectral function of ^{3}He, obtained by using the Argonne v14 NN potential [21] and the Coulomb interaction (see text), vs. the removal energy E and the nucleon momentum $p \equiv |\vec{p}|$. The deuteron channel is not presented.

Fig. 1(b). The function $\mid B^p_{1,\frac{1}{2}} \mid$, obtained by using the Argonne v14 NN potential [21] and the Coulomb interaction (see text), vs. the removal energy E and the nucleon momentum $p \equiv |\vec{p}|$.

Fig. 1(c). The function $\mid B^p_{2,\frac{1}{2}} \mid$, obtained by using the Argonne v14 NN potential [21] and the Coulomb interaction (see text), vs. the removal energy E and the nucleon momentum $p \equiv |\vec{p}|$.

Fig. 2(a). The same as Fig. 1(a), but for the neutron.

Fig. 2(b). The same as Fig. 1(b), but for the neutron.

Fig. 2(c). The same as Fig. 1(c), but for the neutron.

Fig. 3(a). The asymmetry of ^{3}He corresponding to $\epsilon_1 = 370\ MeV$, $\theta_e = -91.4^o$ and $\beta = 42.5^o$, vs. the energy transfer ν, calculated with different two-body interactions. Solid line: Av14 + Coulomb interaction; dashed line: RSCv8 + Coulomb interaction; dotted line: Paris potential without Coulomb interaction, after [9]. Dot-dashed line: the neutron contribution for the Av14 + Coulomb interaction case. The nucleon form factors of Ref. [27] have been used. The arrow indicates the position of the qe peak, where one has $\theta^* \simeq 8.9^o$ and $Q^2 = 0.19\ (GeV/c)^2$. The experimental data are from Ref. [5].

Fig. 3(b). The same as Fig. 3(a), but for different three-body interactions. Solid line: Av14 + Coulomb interaction; dashed line: the Brazil three-body force [23] has been added to Av14 + Coulomb interaction; dotted line: the same as the dashed line, but for the Tucson-Melbourne three-body force [24]. The three curves largely overlap for both the total asymmetry and the neutron contribution.

Fig. 4(a). The same as Fig. 3(a), but for $\theta_e = 70.1^o$. The experimental data are from Ref. [6]. The arrow indicates the position of the qe peak, where one has $\theta^* \simeq 87^o$ and $Q^2 = .14\ (GeV/c)^2$.

Fig. 4(b). The same as Fig. 3(b), but for $\theta_e = 70.1^o$.

Fig. 5(a). The functions $\mathcal{H}^n_{T'(TL')}(Q^2, \nu_{peak})$ for the neutron in ^{3}He (see Eq. (21)) vs Q^2, and the corresponding approximation $\mathcal{F}^{\ni\mathcal{H}],\backslash}_{\mathcal{T}'(\mathcal{T}\mathcal{L}')}\left(\mathcal{Q}^{\in}, \nu_{\sqrt{\ }^{]\dashv\|}}\right)$ (see Eqs. (22) and (23)). All the curves have been obtained from the Av14 + Coulomb interaction and the nucleon form

factors of Ref. [27]. Solid line: $\mathcal{H}^n_{T'}(Q^2,\nu_{peak})$; dot-dashed line: $\mathcal{H}^n_{TL'}(Q^2,\nu_{peak})$; dashed line: $\mathcal{F}^{\ni\mathcal{H}],\setminus}_{\mathcal{T}'}$ (see Eq.(22)); dotted line: $\mathcal{F}^{\ni\mathcal{H}],\setminus}_{\mathcal{TL}'}$ (see Eq.(23)). The curves largely overlap and can be hardly singled out.

Fig. 5(b). The same as Fig. 5(a), but for proton in ^{3}He.

Fig. 5(c). The same as Fig. 5(a), but for proton in ^{3}H.

Fig. 5(d). The same as Fig. 5(a), but for neutron in ^{3}H.

Fig. 6(a). The ratio $R^{^3He}_{T'}(Q^2,\nu_{peak})/G^2_D(Q^2)$ (see Eq. (10)) vs Q^2 ($G_D(Q^2)=1/(1+Q^2/0.71)^2$). Solid line: the response $R_{T'}$ obtained from the Av14 + Coulomb interaction; dot-dashed line: the same as the solid line, but without Coulomb interaction, (this line largely overlaps with the solid one); dotted line: the same as the solid line, but for RSCv8 potential; dashed line: the three-body interaction [23, 24] has been added to Av14 + Coulomb interaction (the Brazil [23] and the Tucson-Melbourne [24] three-body interactions essentially yield the same results).

Fig. 6(b). The same as Fig. 6(a), but for the response $R^{^3He}_{TL'}(Q^2,\nu_{peak})$ (see Eq. (11)).

Fig. 6(c). The ratios $R^{^3He,p}_{TL'}(Q^2,\nu_{peak})/R^{^3He}_{TL'}(Q^2,\nu_{peak})$ and $R^{^3He,p}_{T'}(Q^2,\nu_{peak})/R^{^3He}_{T'}(Q^2,\nu_{peak})$ vs. Q^2, at the qe peak. The lines are the same as in Fig. 6(a).

Fig. 7(a). The same as Fig. 6(a), but for ^3H. Solid line: the response $R_{T'}$ obtained from the Av14 interaction; dotted line: the same as the solid line, but for RSCv8 potential; dashed line: the three-body interaction [23, 24] has been added to Av14 interaction (the Brazil [23] and the Tucson-Melbourne [24] three-body interactions essentially yield the same results).

Fig. 7(b). The same as Fig. 7(a), but for the response $R^{^3H}_{TL'}(Q^2,\nu_{peak})$ (see Eq. (11)).

Fig. 7(c). The same as Fig. 6(c), but for neutron in ^3H. The lines are the same as in Fig. 7(a).

Fig. 8. The ratio $R^{^3He}_{TL'}(Q^2,\nu_{peak})/K^p_{TL'}$, with $K^p_{TL'}=-2\sqrt{2}G^p_EG^p_M$, vs. Q^2 (see text) . The solid line represents the calculation obtained by using in Eq.(11) the spin-dependent spectral function corresponding to Av14 + Coulomb interaction and the Galster nucleon form factors [27]. Dot-dashed line: the ratio $R^{^3He,p}_{TL'}/K^p_{TL'}$, corresponding to the proton contribution, has been shown as reference line.

Fig. 9. The polarization angle β_{critic}, where the proton contribution to the polarized cross section of ^{3}He, at the qe peak, vanishes, vs. Q^2 (see Eq.(3)). Solid line: Av14 + Coulomb interaction; dashed line: Av14 + Coulomb interaction + three-body forces; dotted line: RSCv8 + Coulomb interaction (the Brazil [23] and the Tucson-Melbourne [24] three-body interactions yield essentially the same results). The nucleon form factors [27] have been used.

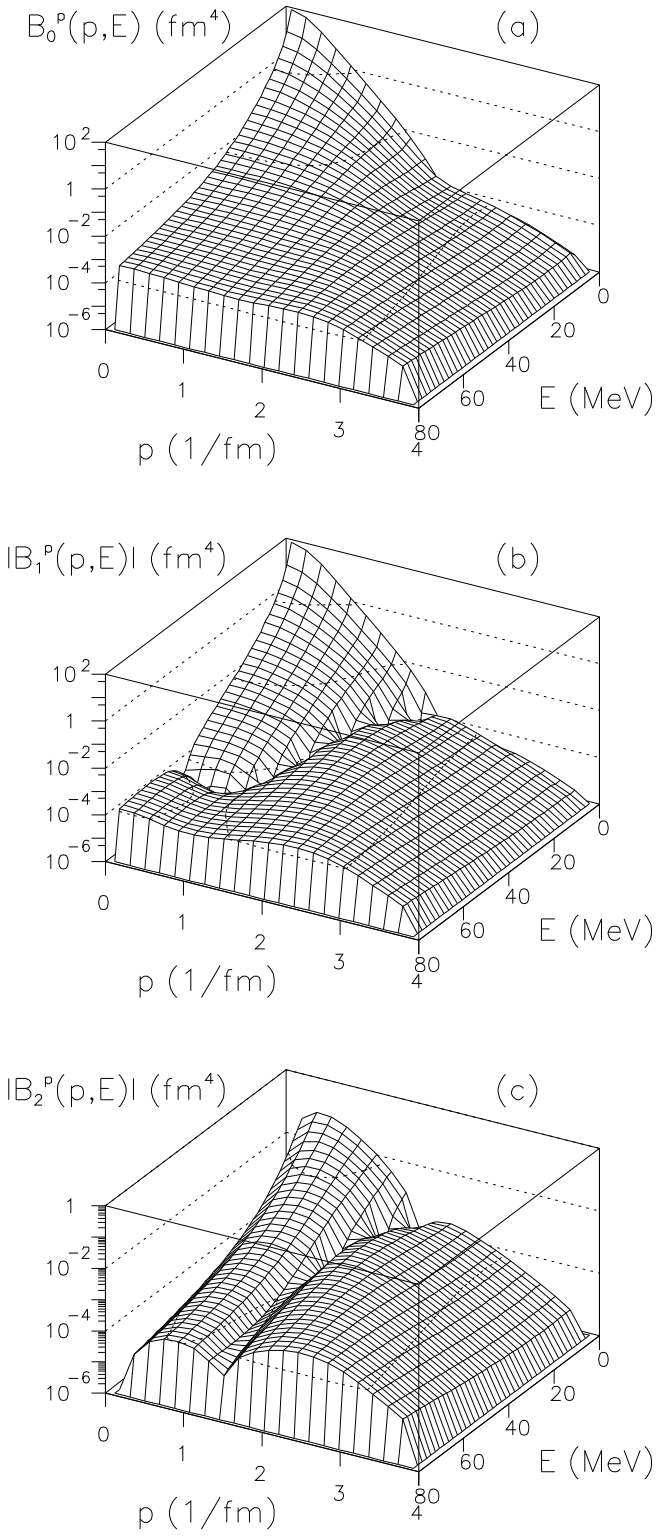

Fig. 1 - A. KIEVSKY, M. VIVIANI, E. PACE and G. SALME'

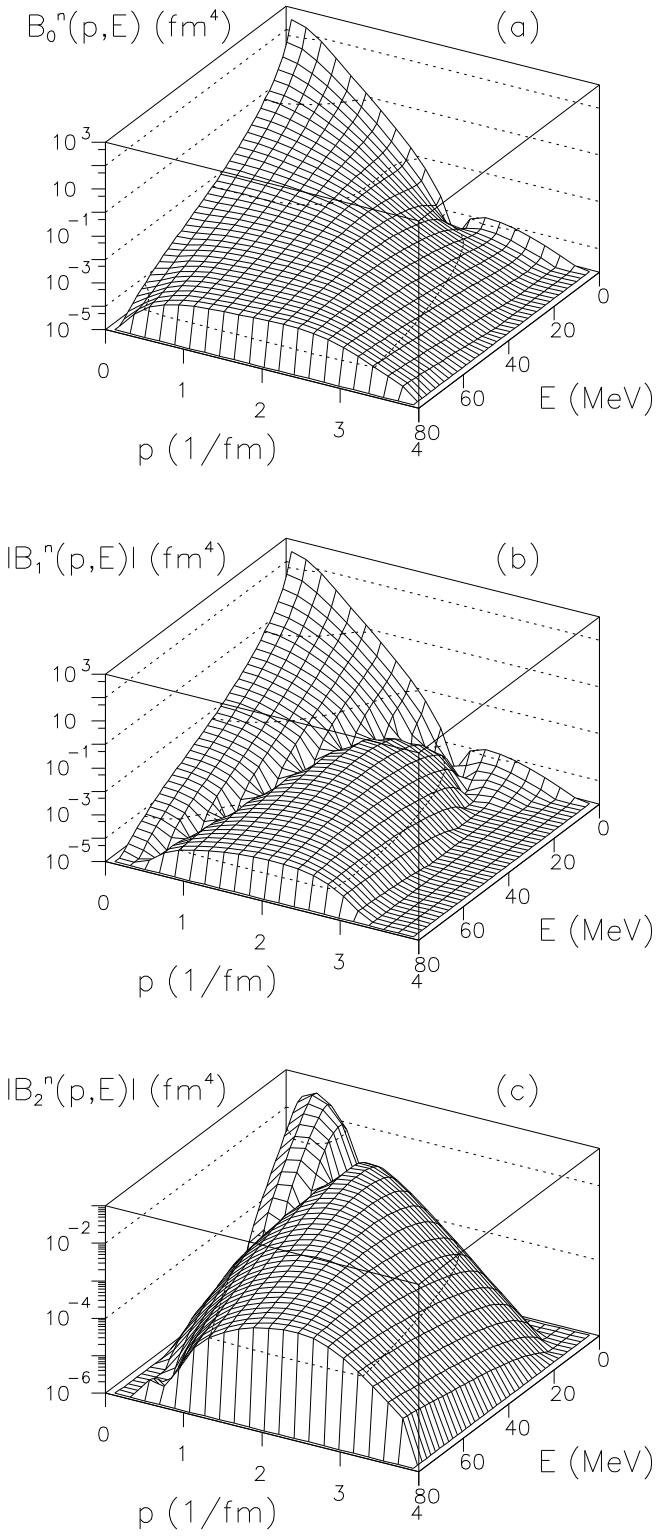

Fig. 2 - A. KIEVSKY, M. VIVIANI, E. PACE and G. SALME'

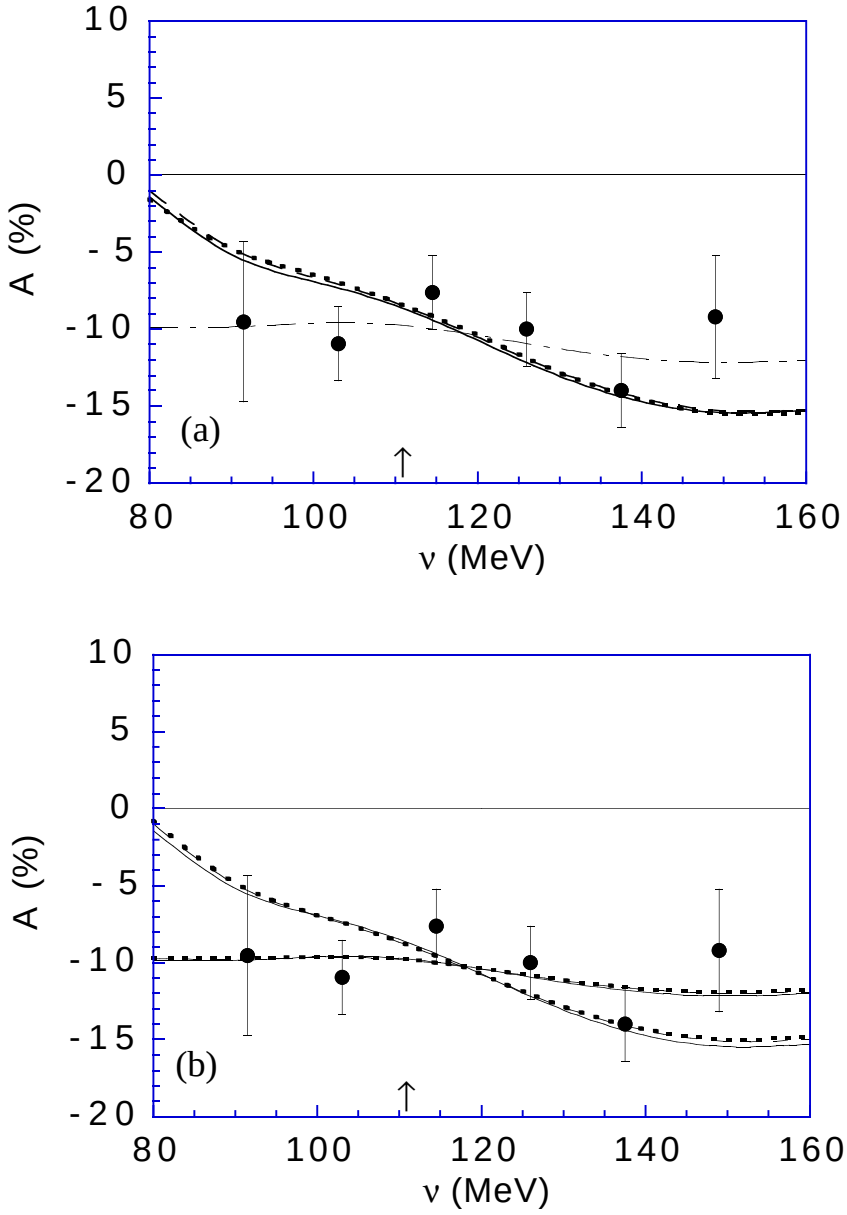

Fig. 3 - A. KIEVSKY, M. VIVIANI, E. PACE and G. SALME'

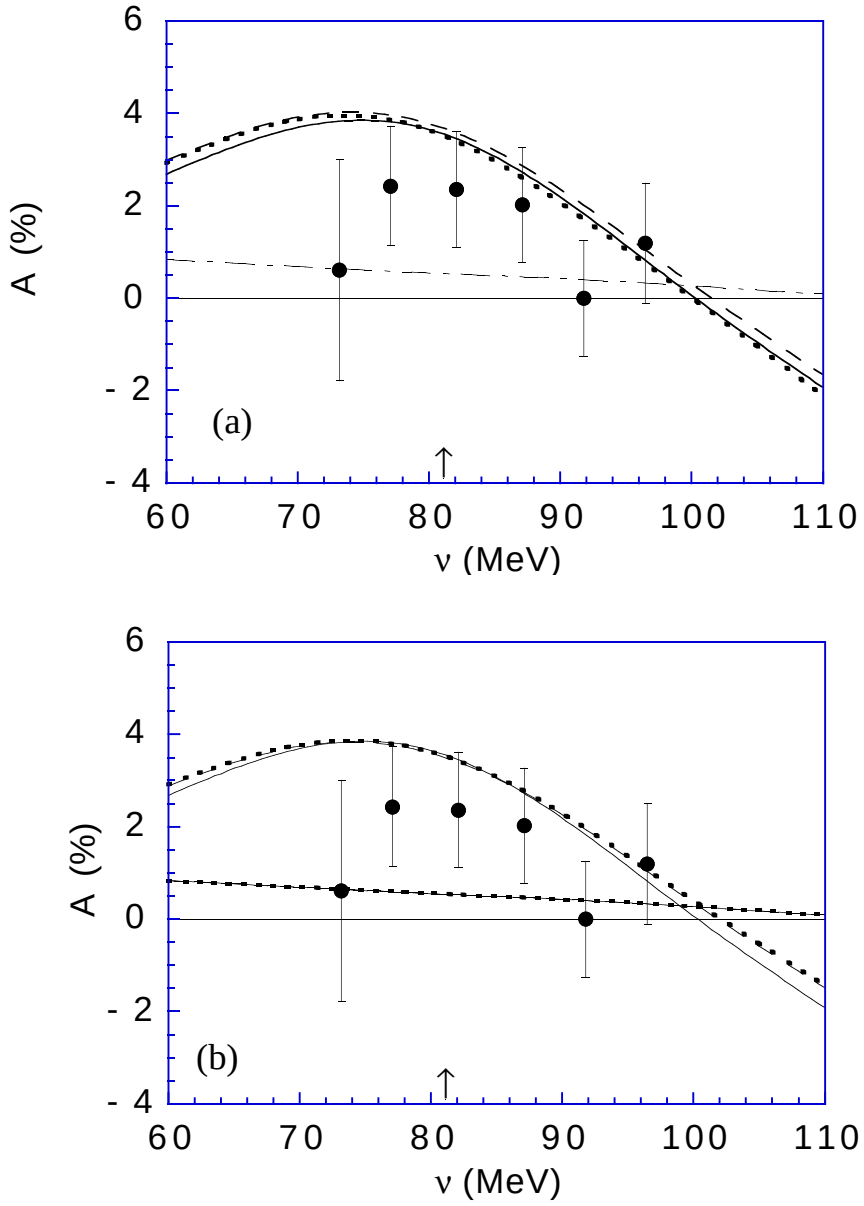

Fig. 4 - A. KIEVSKY, M. VIVIANI, E. PACE and G. SALME'

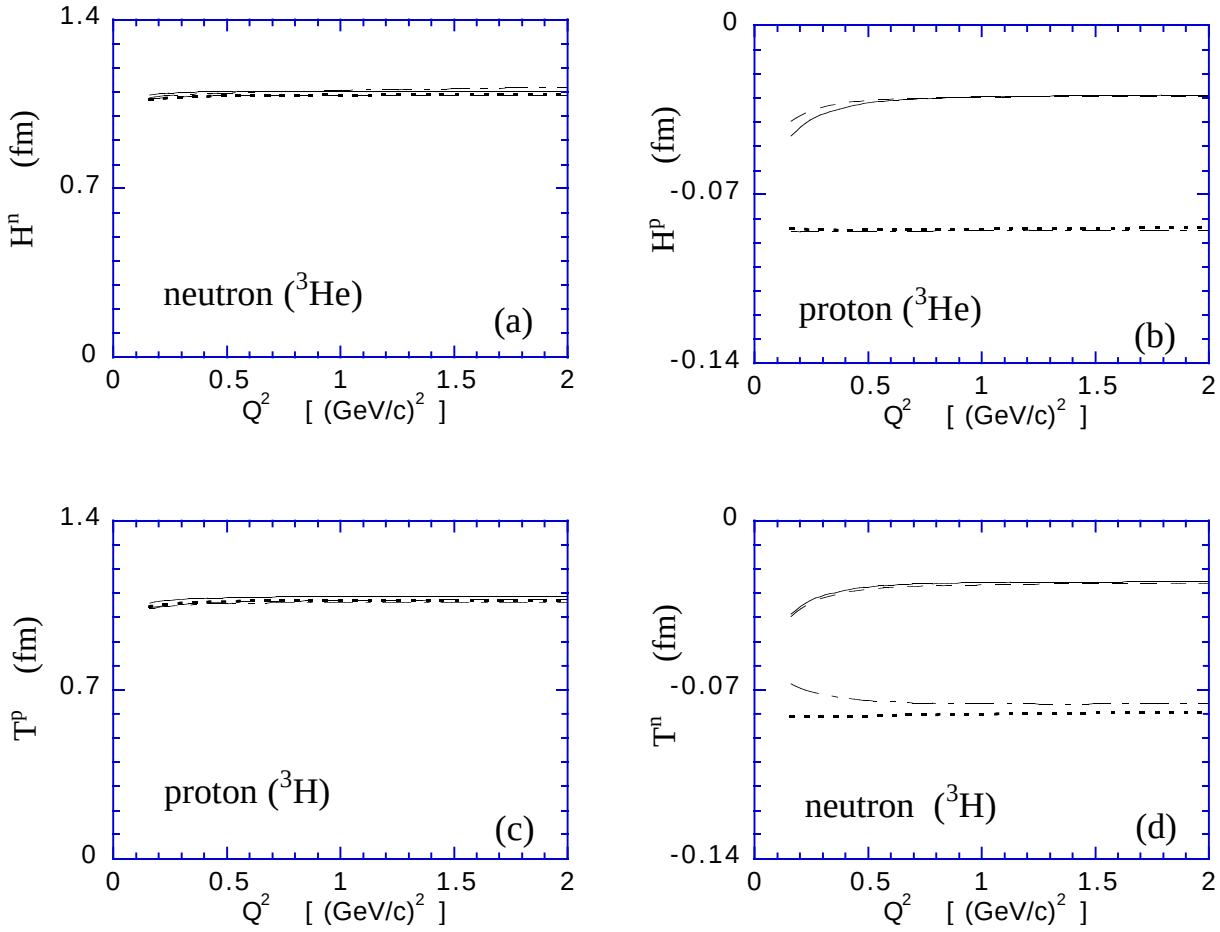

Fig. 5 - A. KIEVSKY, M. VIVIANI, E. PACE and G. SALME'

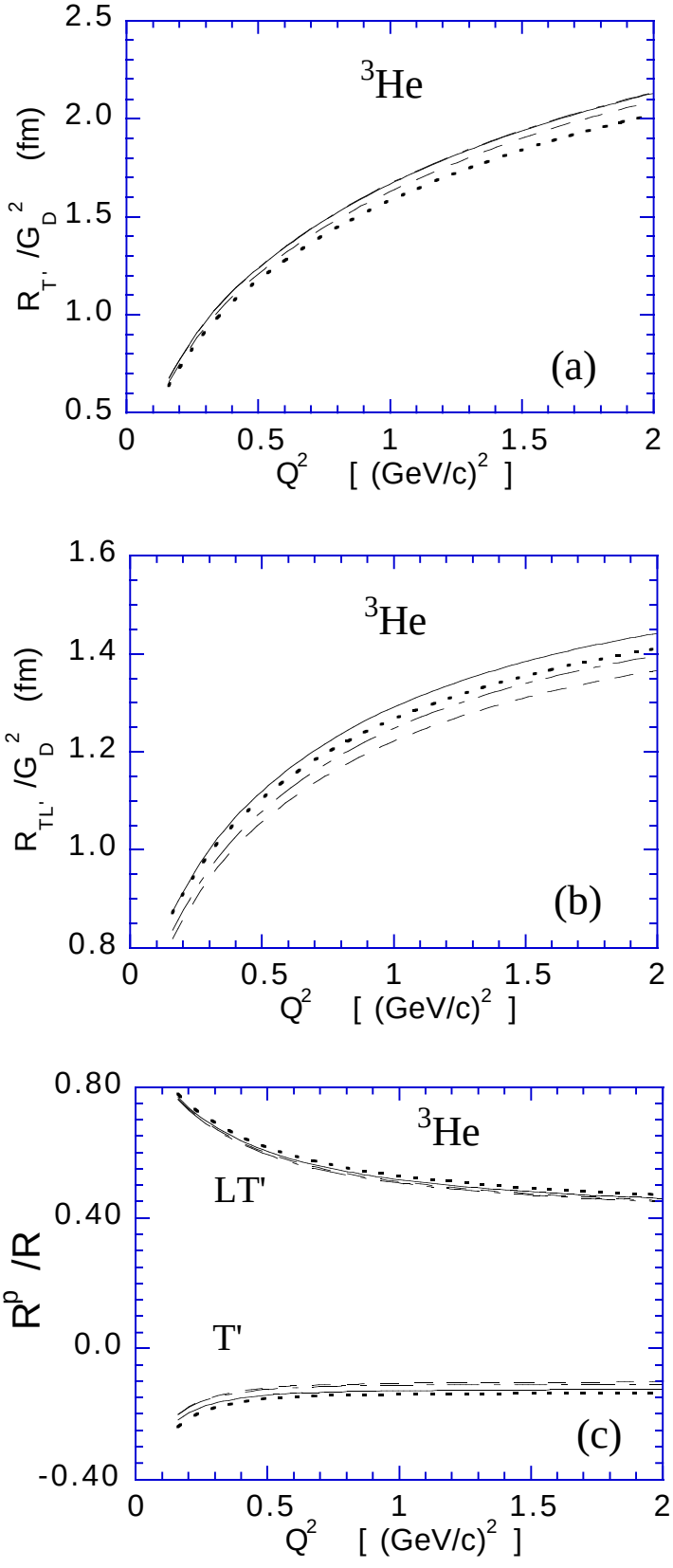

Fig. 6 - A. KIEVSKY, M. VIVIANI, E. PACE and G. SALME'

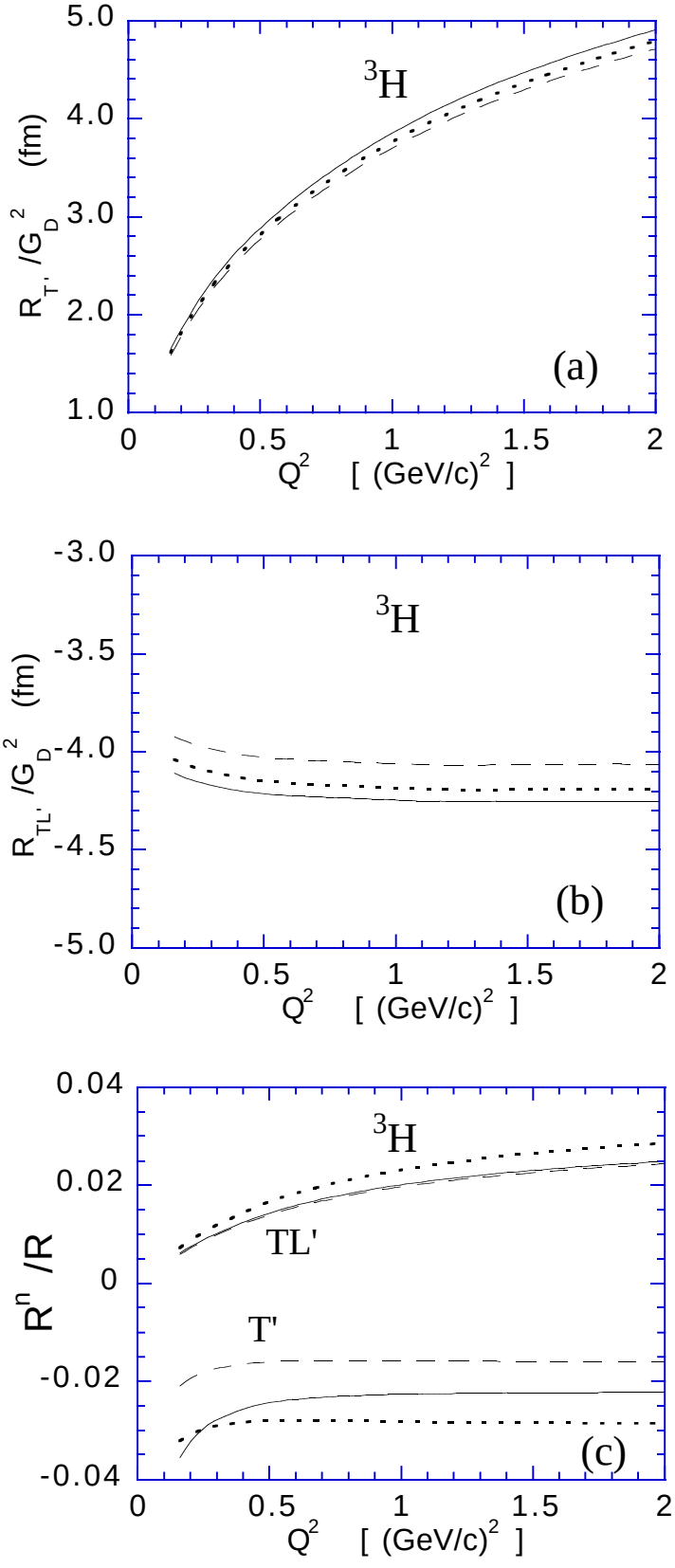

Fig. 7 - A. KIEVSKY, M. VIVIANI, E. PACE and G. SALME'

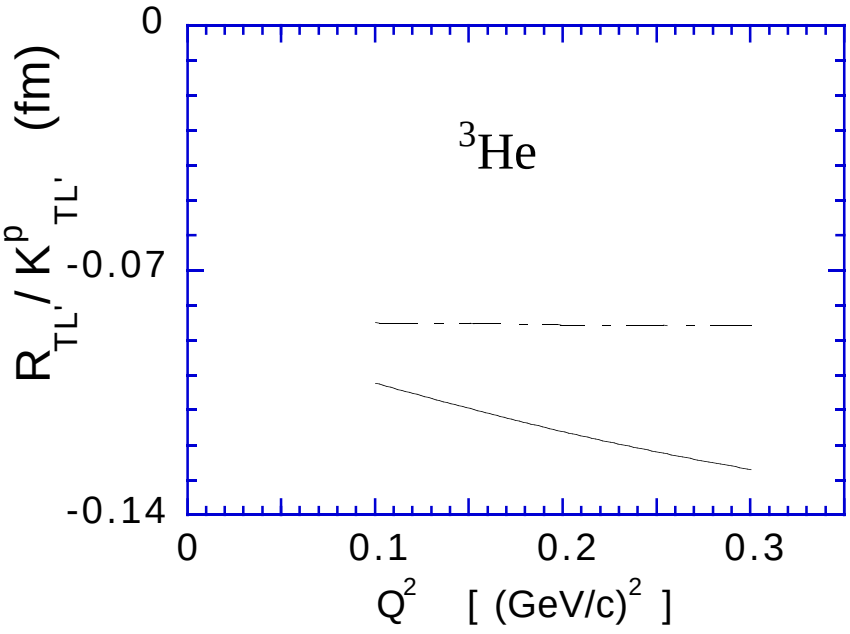

Fig. 8 - A. KIEVSKY, M. VIVIANI, E. PACE and G. SALME'

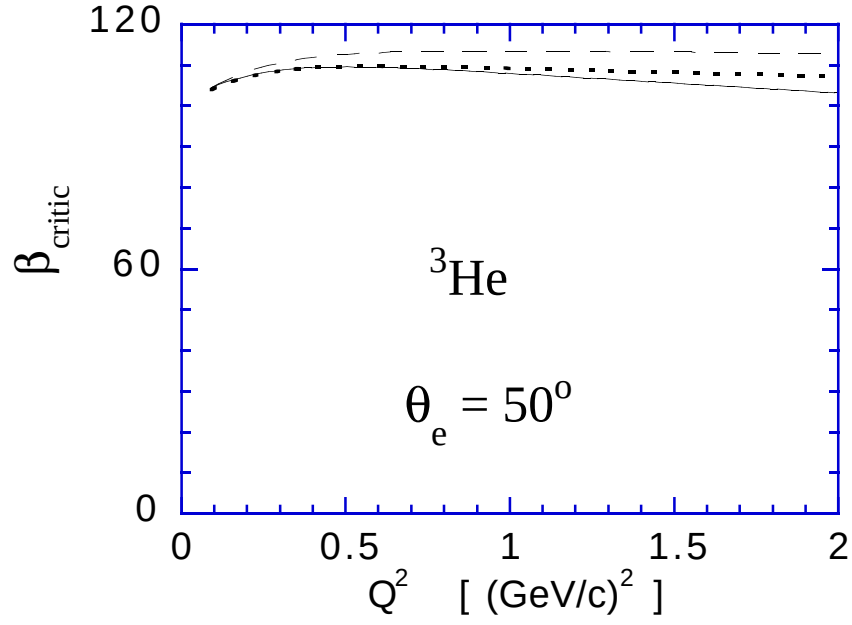

Fig. 9 - A. KIEVSKY, M. VIVIANI, E. PACE and G. SALME'